MTPV Flux-Weakening Strategy for PMSM High Speed Drive

Léopold Sepulchre, Maurice Fadel, Maria Pietrzak-David, Guillaume Porte

MTPV Flux-Weakening Strategy for PMSM High Speed Drive

Léopold Sepulchre, Maurice Fadel, Maria Pietrzak-David and Guillaume Porte

***Abstract*—High speed permanent magnet synchronous motors (PMSMs) are used in electric vehicles because of their intense power density. The high speed implies a significant electromotive force and requires flux weakening. The usual control algorithms realize flux weakening by adding a negative I_d current component when the voltage required by the current regulation exceeds the maximum voltage depending on the battery. If the magnet can be totally defluxed, then it is better to use a maximum torque per volt strategy. Furthermore, there is no speed regulation in the control and the driver gives a torque reference. This reference value has to be limited by the attainable operating points; therefore, the battery power limit has to be taken into account in addition to the voltage and current limits. The *d–q* current references are calculated to minimize the total current magnitude required to reach the reference torque. This paper proposes a strategy to control a PMSM operating continuously since the speed zero up to the maximum speed without the switching algorithm, in order to take into account the different limitations (current, voltage, and power) and to expand the overspeed zone. In order to validate the proposed strategy, experimental results are shown for a low power machine.**

***Index Terms*—Flux weakening, high speed permanent magnet synchronous motor (PMSM), maximum torque per volt (MTPV), torque–speed characteristic, vector control.**

NOMENCLATURE

LPF	Low-pass filter.
MinCPT	Minimal current per torque.
MTPA	Maximum torque per ampere.
MTPV	Maximum torque per volt.
PMSM	Permanent magnet synchronous motor.
PWM	Pulsewidth modulation.
SCR	Single current regulator.
LUT	Lookup tables.
TFC	Torque and flux control.
UDFVC	Unified direct flux vector control.
VCC	Vector current control.

I. INTRODUCTION

ELECTRIC vehicles are the present and the future of the automobile industry because they are environment friendly: low noise levels, better performances than thermal engines, and electrical energy is cheaper than oil-based fuel. So, electrical traction requires motors to have a high torque at low speeds and a wide speed range at constant power.

PMSMs are commonly used because this electrical motor has the best power density and efficiency to date [1] and is therefore well adapted for embedded applications. The volume and mass of a PMSM are proportional to its torque. An engine containing fewer magnets making it smaller, lighter, and cheaper has been chosen, thereby improving volume and mass. It has less torque but the same power because it operates at higher speeds and the gear can be adapted to the desired torque–speed characteristics, thereby retrieving the qualities of electrical traction. The motor is supplied from a battery through, a three-phase voltage-source inverter (VSI). The control is performed in the Park *d–q* reference frame. The torque reference is imposed from the accelerator, allowing a calculation of the *d–q* current references. Motor *d–q* currents are regulated by two discrete polynomial controllers with a decoupling strategy and the consideration of delays [2]. A PWM strategy generates the duty cycles sent to the VSI power components. When the speed increases, the electromotive force of the machine increases also, and, because of the battery voltage limit, from a certain speed the magnet flux perceived by the stator windings must be reduced. This is done by imposing a negative I_d current that will generate an opposing flux to that of the magnet flux. This process is called flux weakening.

The literature presents several flux-weakening control strategies [3]–[24], where [3]–[5] are the state of the art in flux-weakening techniques. We suggest classifying these strategies in the following way: analytical direct calculation method [6], [7], direct open loop algorithm with experimental LUT [8]–[11], SCR method [4], [12]–[14], TFC method with LUT [15], [16], UDFVC in the stator flux frame [17], [18], and VCC [15],

[19]–[25]. This last method is divided into: regulation on the voltage magnitude [15], [19]–[22], regulation on the voltage error [4], [15], [23], regulation on the current error [15], [24], and regulation on the duty cycle [15], [25]. If the magnet can be totally defluxed, i.e., the critical point is within the current limit, then an MTPV is required for flux weakening [4]–[7], [12]–[14], [17], [26]–[30]. The analytical direct open-loop calculation method [7], [26], [27], direct open-loop experimental LUT [4]–[7], [28], SCR method [12]–[14], and UDFVC [17] enable MTPV flux weakening [29], [30] using the VCC strategy associated with MTPV but they also require an algorithm switch. The open-loop method with direct calculation from the motor equations is very sensitive with regard to parameter variation. For salient-pole PMSM, this method needs long calculations in real-time controls and also to define torque references. LUT working in open loop or TFC operating in closed loop are adapted for taking into account the inductance of magnetic saturation. This depends on the motor and previous experimental tests have to be carried out. In a voltage saturation operation, the SCR avoids competition between the classic *d*-axis and *q*-axis regulators but this method requires switching to another control algorithm at low speeds. The UDFVC is compatible for all ac machines; however, it requires the use of a flux observer. Furthermore, the maximum load torque has to be determined experimentally which renders this method dependent on the motor. VCC is the classic flux-weakening method. Nevertheless in the current control, the LPF impacts its dynamic performances. The voltage and the regulation of the duty cycles also use LPF with the same consequences. There are overmodulation strategies that increase the maximum voltage available at the expense of additional current harmonics. Finally, the voltage norm regulation is the conventional approach that needs a maximum voltage reference depending on the battery and PWM used to overmodulate. The control developed in this paper is based on this approach. The proposed solution relies on the implementation of an MTPV method taking into account a power limit of the energy source, working continuously from a rotation speed of zero to its maximum value.

It can be noted that the reachable operating points are dependent on the maximum current and voltage and on the power of the battery. In Section II, these limits are discussed and plotted in the torque–speed plane. The previously mentioned flux-weakening strategies usually do not take into account the power limit and only consider the current and voltage limits. This paper proposes an algorithm to calculate the optimal components of the current in *d–q* frame for smooth-pole or salient-pole PMSM. It takes into account the physical limitations of the system (maximum current, maximum voltage, maximum power), in order to operate continuously since the zero speed to the maximum speed without the switching algorithm and to maximize the overspeed zone. The performance of this solution is observed through simulation and validated with experimental bench.

II. Achievable Operating Points

A. PMSM Model and Electric Limits

The PMSM electrical model equations, expressed in the *d–q* reference frame, are presented for voltage (1) and (2) and for the torque (3)

$$V_d = R \cdot I_d + L_d \frac{dI_d}{dt} - \omega \cdot L_q \cdot I_q \tag{1}$$

$$V_q = R \cdot I_q + L_q \frac{dI_q}{dt} + \omega \cdot L_d \cdot I_d + \omega \cdot \varphi_f \tag{2}$$

$$T = \frac{3}{2} \cdot p \cdot (\varphi_f \cdot I_q + (L_d - L_q) I_d I_q) \tag{3}$$

where V_d, V_q and I_d, I_q are, respectively, the voltage and current *d–q* components, L_d and L_q are the *d* and *q* axes winding inductances, p is the number of pair of poles, ω presents the electrical rotor angular velocity, R is the phase resistance, Φ_f is the linkage flux of the permanent magnet, and T corresponds *to* the PMSM electromagnetic torque.

The maximum current $I_{\max}$ (4) is the more constraining current limit which is situated between the nominal current of the motor, the nominal current of the inverter, and the maximum current delivered by the battery (brought back to an equivalent motor current)

$$\sqrt{I_d^2 + I_q^2} \leq I_{\max}. \tag{4}$$

The maximum voltage (5) depends on the voltage limit of the battery and the PWM strategy used; for the space vector modulation (SVM) applied here, $V_{\max}$ is defined by (6)

$$\sqrt{V_d^2 + V_q^2} \leq V_{\max} \tag{5}$$

$$V_{\max} = \frac{V_{\mathrm{DC}}}{\sqrt{3}} \tag{6}$$

where V_{DC} is the voltage of the battery.

At high operating speed, the resistance is usually negligible in (1) and (2). Consequently, the voltage limit can be written in steady state as follows:

$$\sqrt{(\omega L_q I_q)^2 + (\omega L_d I_d + \omega \varphi_f)^2} \leq V_{\max}. \tag{7}$$

B. Torque–Speed Characteristic in Electrical Traction

A reduced size salient-pole PMSM is used to perform the experiments and the simulations. Its parameters are displayed in Table I.

TABLE I
PMSM Parameters

Reduced size salient pole PMSM parameters	
R	0.97 Ω
L_d	4.73 mH
L_q	5.77 mH
Φ_f	0.0345 Wb
P	5
I_{max}	8 A
V_{DC}	200 V
Power battery 1 C10=70Ah	1400 W
Power battery 2 C10=100Ah	1000 W

To operate, the vehicle requires a high torque available at low speeds and with constant power for wide rotation speed ranges. Fig. 1 shows the maximum torque attainable according to speed and under nominal conditions for different control strategies. It corresponds to smooth-pole PMSM whose parameters are

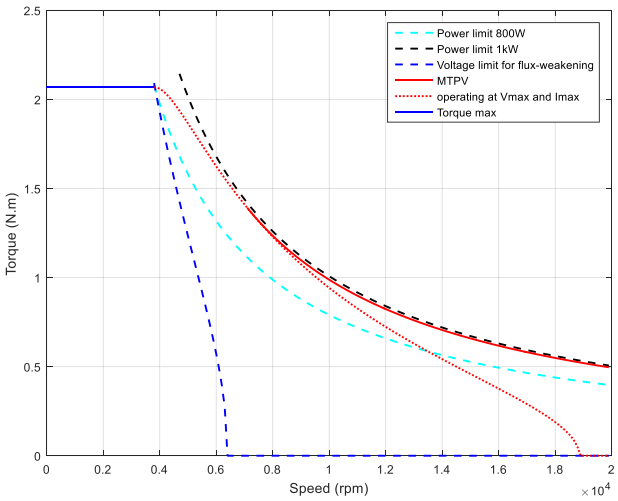

Fig. 1. Torque–speed characteristics of the smooth-pole PMSM from Table I.

similar to those in Table I, but with L_d equal to L_q. The flux-weakening operation allows the curve of maximum power to be reached, by acting on the axis d by injecting a current according to a law as explained next.

The blue solid line in Fig. 1 shows the maximum torque at low speed that is given by the MTPA strategy with maximum current expressed by (8) and (9). Note that the voltage limit is not yet reached, so the operating points below the torque limit are imposed by the control which minimizes the current corresponding to the reference torque in order to reduce the PMSM losses. If this strategy is maintained when the speed increases, then when the voltage limit is reached, it gives the blue-dashed line torque limit explicit in (12), and flux weakening will need to be done to reach operating points at higher speeds. It can be noted that, depending on the sizing of the inverter, the current limit and consequently the torque limit can be lower at speeds near zero in steady state but this case is not discussed here. The MTPA expression in the torque–speed plane is (3) with (8) and (9) with the torque reference represented by its equivalent current norm I_{norm}. With the help of the Lagrange multiplier [33] method, it is easy to formulate the following expressions:

$$I_d = \frac{\varphi_f - \sqrt{\varphi_f^2 + 8(L_d - L_q)^2 I_{\text{norm}}^2}}{-4(L_d - L_q)} \tag{8}$$

$$I_q = \sqrt{I_{\text{norm}}^2 - I_d^2} \tag{9}$$

where I_{norm} is the total current magnitude and depends on the torque reference or speed regulation. Note that for smooth-pole PMSM, the classic MTPA d and q current references are obtained as follows:

$$I_d = 0 \tag{10}$$

$$I_q = I_{\text{norm}}. \tag{11}$$

The expression of the voltage limit in the torque–speed plane without flux weakening for a smooth-pole PMSM is (3) with (10) and (12). For a salient-pole PMSM, the MTPA strategy already adds some I_d current and so the expression of the torque depending on the speed and on the voltage limit is (3) with I_d solution of (22) and I_q respects (7)

$$I_q = \sqrt{\left(\frac{V_{\max}}{L_q \omega}\right)^2 - \left(\frac{\varphi_f}{L_q}\right)^2}. \tag{12}$$

The red-dotted line in Fig. 1 plots the maximum torque that can be achieved if the voltage limit and the current limit are reached, expressed in (13)–(15). When the speed increases, the electromotive force becomes more restrictive for the voltage. To respect the voltage limit, the flux perceived by the stator winding has to be reduced. In this way, a negative I_d current is applied that creates a flux opposite to the magnet flux: this is the flux weakening. Note that the operating points below this torque limit are imposed by the controller with a classic flux-weakening algorithm, i.e., VCC that will follow the intersection between the current and the voltage limits. It can also be seen that the torque–speed characteristic is not really a constant power limit if only the current and voltage limits defined in (4) and (7) are considered especially in the "top right corner" where the torque is high and the voltage limit is just reached. The classic power limit is mainly a battery limit or a mechanical requirement rather than an electric motor limit.

For a smooth-pole PMSM, the direct current component is as follows:

$$I_d = \frac{V_{\max}^2 - \omega^2 \varphi_f^2 - L_q^2 \omega^2 I_{\max}^2}{2 L_d \omega^2 \varphi_f}. \tag{13}$$

For a salient-pole PMSM, this current is expressed by

$$I_d = \frac{L_d \varphi_f}{L_d^2 - L_q^2} + \frac{\sqrt{L_d^2 \varphi_f^2 - (L_d^2 - L_q^2)\left(\varphi_f^2 + L_q^2 I_{\max}^2 - \frac{V_{\max}^2}{\omega^2}\right)}}{L_d^2 - L_q^2} \tag{14}$$

and

$$I_q = \sqrt{I_{\max}^2 - I_d^2}. \tag{15}$$

The solid red line in Fig. 1 shows the MTPV, explicit in (16) and (17). This magnet must be able to be totally defluxed. It is possible when the critical point is within the current limit. In this case, this strategy gives the highest torque at high speed. The control strategy in Section III presents a way to include MTPV in a flux-weakening method. Note that in such a case the speed is theoretically not limited by the electrical limits. The MTPV expression in the torque–speed plane is (3) with (16) and (17). By injecting the relation (16) and (17) into the expression (3) and using the Lagrange multiplier method again, we can express V_d and V_q voltages which correspond to the MTPV strategy. So, the d and q current components are as follows:

$$I_d = \frac{\left(\frac{V_q}{\omega} - \varphi_f\right)}{L_d} \tag{16}$$

$$I_q = -\frac{V_d}{L_q \omega}. \tag{17}$$

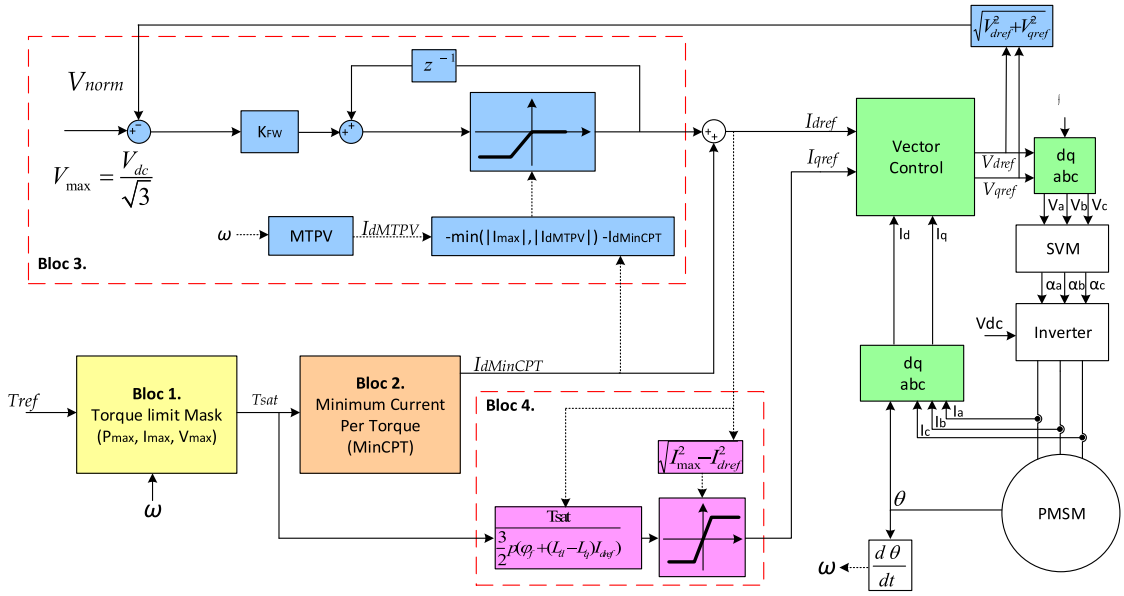

Fig. 2. Scheme of the PMSM control (where AW is a structural antiwindup).

It should be noted that this approach gives two solutions. We chose the one that gives negative I_d and positive I_q

$$V_q = \frac{\varphi_f - \sqrt{{\varphi_f}^2 + V_{\max}^2 8\left(\frac{L_d - L_q}{L_q \omega}\right)^2}}{-4\left(\frac{L_d - L_q}{L_q \omega}\right)} \tag{18}$$

$$V_d = -\sqrt{V_{\max}^2 - V_q^2}. \tag{19}$$

For nonsalient-pole PMSM, the MTPV references become

$$I_d = \frac{-\varphi_f}{L_d} \tag{20}$$

$$I_q = \frac{V_{\max}}{L_q \omega}. \tag{21}$$

The black- and cyan-dashed lines in Fig. 1 show two examples of power limits for the battery. For the black-dashed line, the power limit implies a less constraining torque limit than the voltage or current limits and so is not useful for the calculation of the reachable operating points. For the cyan line, the power limit is more constraining than the voltage and current limits and so must be taken into account in the control. Observe that many classic control strategies only consider the voltage and current limitations. The control strategy presented in the next section shows a way to take into account all mentioned limitations to calculate the current references.

III. Flux-Weakening Strategy

This section presents the control strategy that calculates the current references in the d–q reference frame from the torque reference. These current references are applied to the motor current regulation with a decoupling strategy [2]. Other control strategies with high bandwidth can be used for the current regulation, for example, predictive control or optimal control.

The operating limits of the machine are imposed by the limits of its power supply, i.e., the battery. For this, we define a maximum voltage and we also define a maximum current. To maximize the speed of the machine while respecting these constraints, we must define particular current references that generate the maximum torque knowing that for a machine with salient poles the two axes d and q contribute to the torque production.

Fig. 2 shows the scheme of the control with this strategy. The current regulation gives a voltage vector reference. The flux-weakening control compares the norm of this voltage to the voltage limit (6). If this norm is superior to the imposed limit, then a negative I_d current reference is generated to reduce flux seen by the stator windings. Thus, a part of the voltage is liberated and can be used to generate electromagnetic torque. The controller can be synthesized by a cascade method using the closed-loop model of the current regulation (depending on the current regulation used) and positioning the flux-weakening bandwidth accordingly. Nevertheless, it is preferable that the flux-weakening regulation dynamic be negligible according to the mechanical mode and the speed regulation loop if we add one.

The reference torque is limited by a mask (see Fig. 2 Block 1) of the attainable operating points presented in Section II. It enables the control to be reliable to apply a realizable torque respecting all limitations at any rotation speed.

Block 2 of Fig. 2 allows the calculation of the d-current reference and defines the minimal current norm to obtain the limited reference torque, and consequently PMSM losses depending mainly on the current norm. For salient-pole PMSM, I_d current can be calculated by solving (22) obtained by searching the MinCPT

$$I_d^4(L_d - L_q)^3 + I_d^3(L_d - L_q)^2 3\varphi_f + I_d^2(L_d - L_q)3\varphi_f^2 + I_d\varphi_f^3 - \frac{4(L_d - L_q)T_{\text{sat}}}{9p^2} = 0. \tag{22}$$

Using (16), (17), and (5), we can express this equation as a function of $V_{\max}$ and rotation speed ω. This quartic polynomial equation can be solved analytically using the Ferrari method [32]. We can also solve it numerically and establish a LUT of I_d and I_q according to reference torque T_{sat} and speed ω.

For a smooth-pole motor, the solution is trivial (10) but this is not the case of the motor shown in Table I. Classic flux-weakening algorithms use MTPA (8) instead of MinCPT (22). If the power limit of the battery is not constraining (c.f. Section II), then a speed regulation can give a current magnitude divided in current references between the d and q axes by MTPA. Nevertheless, if the power of the battery is constrained, torque information is required in the control to limit this torque or to impose an equivalent current norm limitation induced by the power limitation calculated from (22).

In conclusion, if the motor is with salient poles and the reference torque is imposed or the power battery limit is constraining, then (22) has to be solved; otherwise, an expression (8) can be used as in [31].

It is also possible to inject a negative I_d current that creates an opposite flux to decrease the magnet flux and consequently to liberate all the voltage [c.f. (1) and (2)] for torque generation which follows the MTPV trajectory (16) and (17). This improvement of the control strategy is usually not taken into account in classic controls because it increases the torque only at very high speed and requires totally flux weakening the magnet. In this control, an MTPV strategy is introduced by the modification of the torque limitation (Block 1, in Fig. 2), and by creating a variable saturation in the I_d flux-weakening saturation.

Block 3 in Fig. 2 represents the management of the voltage limit provided by the battery by action on the reference current on the d axis. The limit of the current is defined between the maximum current (4) that is constant and the I_d current required by the MTPV strategy (11) that shortens to the critical point ($I_d = -\Phi_f / L_d$) when the speed increases [31]. For this, it is necessary to act on the limits of the reference current I_d that must take into account the positive effect of the current I_d on the torque produced due to the torque contribution of the saliency.

The regulator of the voltage module uses an integrator with the K_{FW} gain. This gain is calculated empirically to impose a bandwidth of the loop, around 10 rad/s, i.e., ten times faster than the mechanical bandwidth.

The I_q current reference is calculated in Block 4 (see Fig. 2) using (3) with the knowledge of the I_d reference after flux weakening and the limited torque reference. Block 4 also ensures that the final *d–q* current reference is imposed and respects the current limit.

IV. Simulation Results

The performance of the proposed method is observed through a simulation. The PMSM parameters used are shown in Table I. The torque reference is 1.90 N·m and is less than the maximum torque of 2.13 N·m at low speed. We want to analyze the consequences of flux weakening while operating under the current limit, and then observe the PMSM operating in both current and voltage limitations, when the speed increases and more negative I_d current is required.

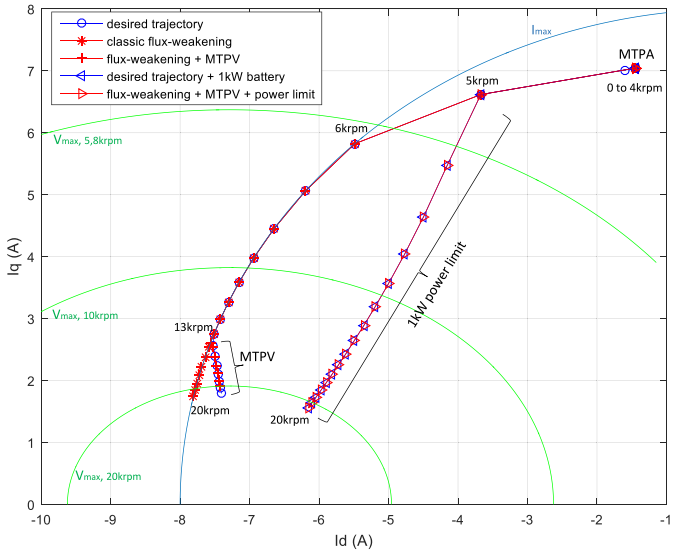

Fig. 3. $I_q - I_d$ scheme of the current references' trajectories.

Fig. 3 shows the current reference trajectory in the $I_d - I_q$ plane. In blue, the current limit (4) is given. There is a circle centered on the origin of the plane and its radius is the norm of the maximum current. In green, the voltage limit (7) is drowning; its form is an ellipse centered on the critical point, and its size decreases when the speed increases. In the blue circles appears desired current reference trajectory in steady-state according to the evolution of the speed computed analytically. These references respect the limitation while generating the required torque with minimal current magnitude at the given speed. The same is true for the blue triangles but with 1-kW battery power that gives a more constraining power limit than the current and voltage limits. In the red stars, the current reference is given with a classic flux-weakening algorithm that only takes into account the current and voltage limits and does not include an MTPV strategy in the control. Note that the current references generated by this algorithm are oversized at high speed and do not respect the battery power limit. The current reference calculated by the flux-weakening control presented in Section III is shown in the red crosses and the same in the red triangles with a 1-kW battery power limit. One can conclude that this algorithm follows the desired current reference trajectory whatever the speed and the constraining limitations. In particular, the cases with operation in MTPV area or power limit are validated.

Figs. 4 and 5 show the torque achieved in steady state for different speeds with a reference torque of 1.90 N·m smaller than its max torque at low rotation speed. Fig. 4 corresponds to the salient-pole PMSM of Table I and Fig. 5 shows for an equivalent smooth-pole PMSM (Table I with L_d equal to L_q). In the blue circles, the torque reference limitation is drawn; it depends on the speed from Section II and in the light-blue triangles, the same variable is shown but with a 1-kW power limit in Fig. 4 and 800 W for Fig. 5. The electrical torque generated with the control in Section III is presented in the red

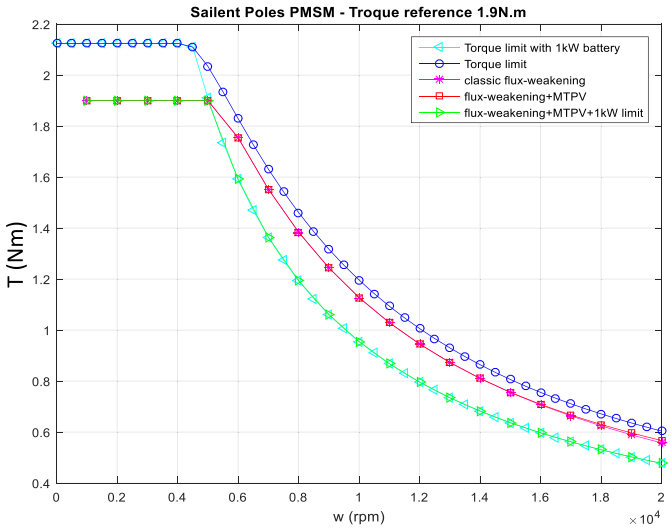

Fig. 4. Torque obtained in steady state depending on the speed with a reference of 1.9 N·m for the salient-pole PMSM from Table I (with 1-kW battery limit).

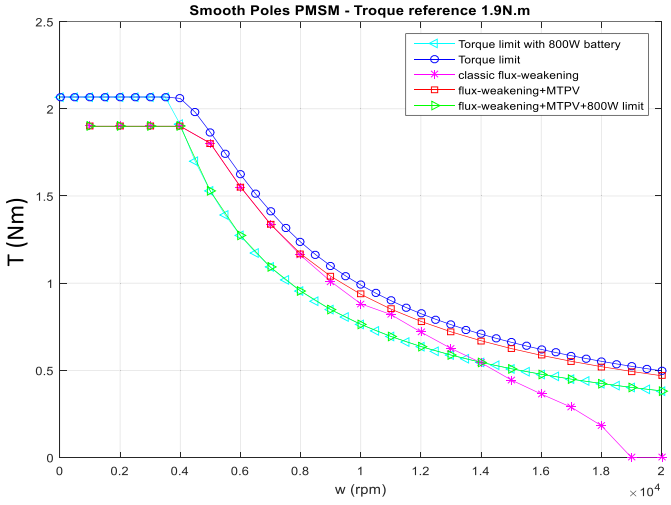

Fig. 5. Torque obtained in steady state depending on the speed with a reference of 1.9 N·m for the smooth-pole PMSM from Table I (with 800-W battery limit).

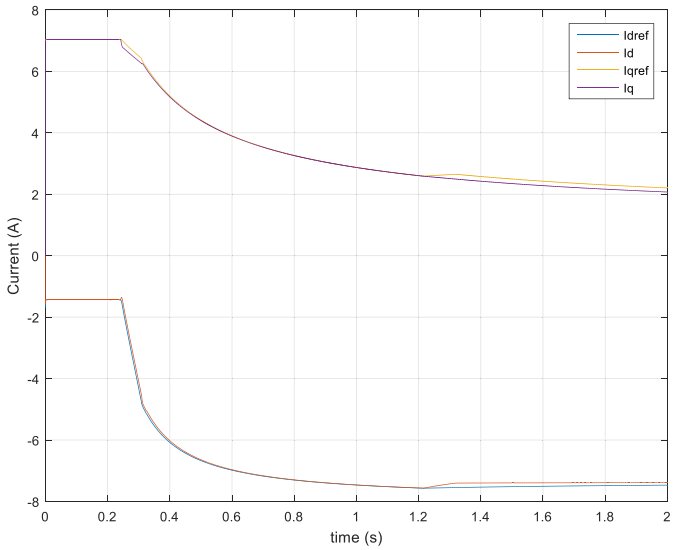

Fig. 6. Torque reference of 1.9 N·m with a 1400-W battery—current I_d and I_q and their references.

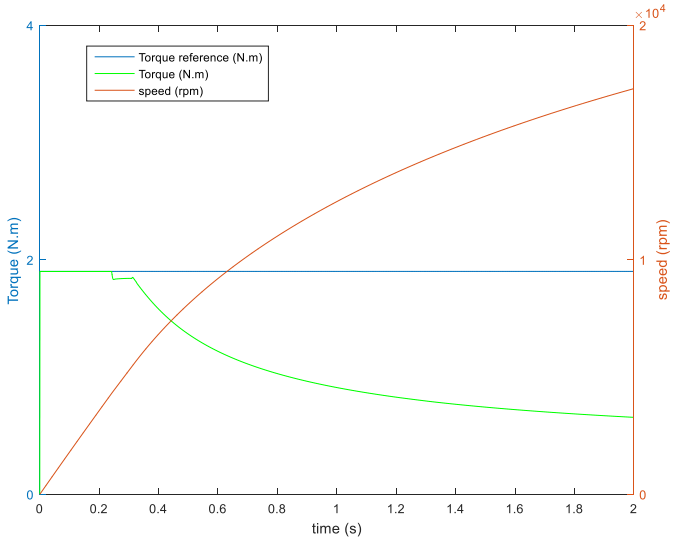

Fig. 7. Torque reference of 1.9 N·m with a 1400-W battery—electromagnetic torque and rotation speed.

squares, and the same variable is given in the green triangles but with a smaller battery with a more constraining power (1 kW for Fig. 4, and 800 W for Fig. 5). It is interesting to note that the power limit is respected even if it is more constraining compared to the other limits. In the magenta stars, the torque generated with classic flux weakening is given with operating for current and voltage limits. One can observe that the MTPV strategy improves performances at high speed because it is not necessary to overly weaken the flux.

It is especially visible in Fig. 5 for the smooth-pole PMSM. For the salient poles motor, the effect of the MTPV strategy is less visible because the I_d negative current for flux weakening also contributes to generating torque. Nevertheless, if it operates at higher speeds, the torque difference would be bigger between the flux-weakening strategy with MTPV and the classic flux-weakening strategy. Finally, the torque error observed in the flux weakening operating between the torque limit and the torque generated is due to the motor resistance that is neglected for the calculation of the theoretical torque limits at high speed but that it still has an impact with the small-scale motor used in this paper.

The following figures show the time simulation results for a torque reference of 1.9 N·m for the salient-pole PMSM with a 1400-W battery. The evolution from the flux-weakening strategy for *d*–*q* current (see Fig. 6), the electrical torque (see Fig. 7), motor rotation speed (see Fig. 8), the voltage norm, and the current norm versus time is displayed. One can recognize the passage of the operating point between the MinCPT area, the flux weakening with only voltage saturation, the flux weakening with both saturation, and the MTPV area when the speed increases.

In Figs. 4 and 5, the different evolutions of the torque are shown. These evolutions correspond to specific trajectories

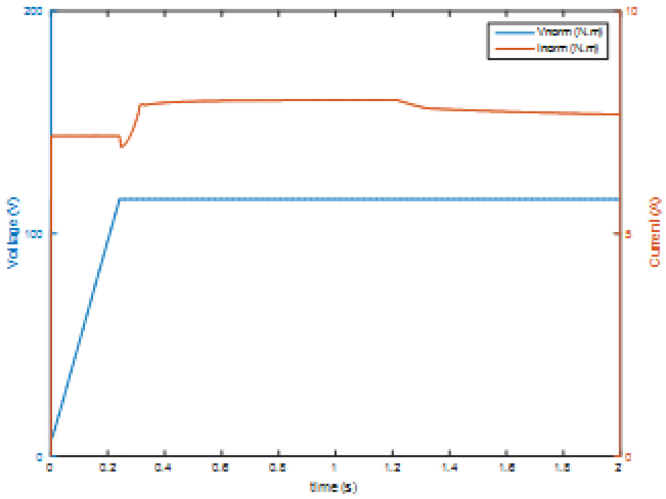

Fig. 8. Torque reference of 1.9 N·m with a 1400-W battery—voltage norm and the current norm.

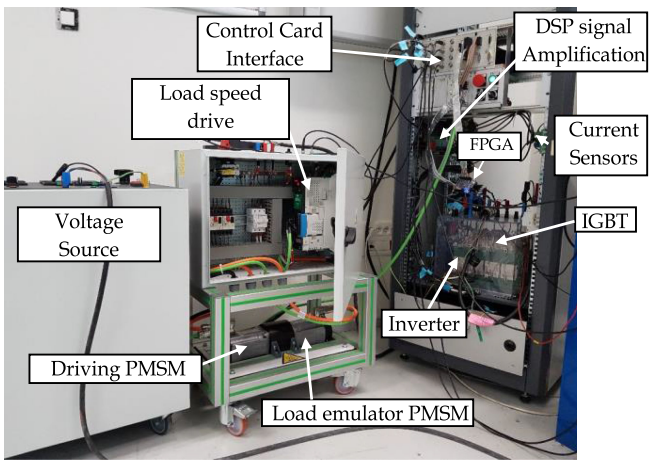

Fig. 9. Bench test of the PMSM propulsion system with load torque emulation.

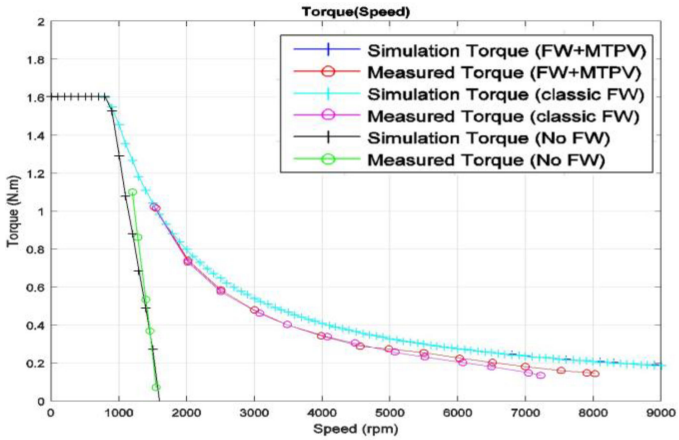

Fig. 10. Mean torque generated with flux weakening + MTPV, with classic flux weakening and without flux weakening (simulation results and experimental tests).

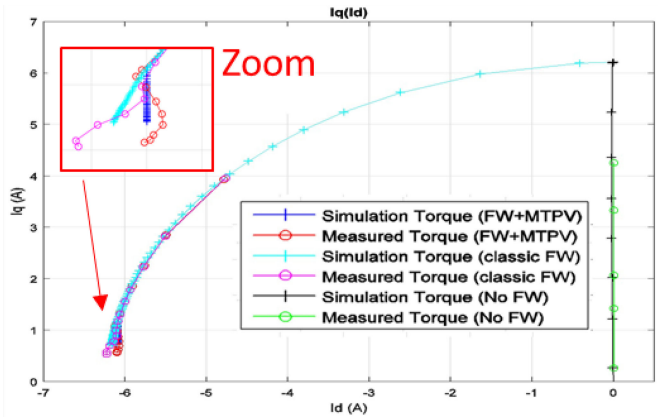

Fig. 11. Experimental and simulation trajectories of average current in the $I_d - I_q$ plane; control algorithms without flux weakening (no FW) and with classic weakening (classic FW), with flux weakening with MTPV.

of the I_d and I_q currents in relation to different strategies (MTPA, MinCPT, MTPV, . . .), which corresponds to the expressions presented in the part II, from (8) to (22). Some of these evolutions are visible in Figs. 3 and 11.

V. Experimental Results

To evaluate the system operation, some experimental tests were realized on the test bench in LAPLACE laboratory shown in Fig. 9. This reduced scale propulsion system is designed with two identical coupled PMSM (parameters given in Table I). One PMSM is the drive motor and the second one can be controlled by imposed load torque or rotation speed and is applied as a load torque emulator. In this way, one can impose the desired load torque to the drive PMSM. The reference torque is imposed by rigorously controlling the current of the loading machine. The torque is not measured but it is known. The VSI operates using an 8-kHz SVM PWM strategy.

The results of the experimental tests are compared with those of the simulation. The corresponding results are shown in Figs. 10–12. It can be noted that the conditions of these tests were the same as in the simulation. Consequently, Fig. 10 compares the mean torque obtained experimentally and by simulation for three control algorithms: without flux weakening, with conventional flux weakening, and also with flux weakening associated with MTPV. Thereby, good concordance is observed between the simulations and the experimental tests in each operating condition.

Fig. 11 shows the current trajectory with the flux-weakening algorithms. We observe that experimental current trajectory correctly follows current saturation up to 5000 r/min.

From 5000 rpm experimental results and simulation results follow to the same direction. These trajectories go toward the critical point of total magnet flux weakening corresponding to I_d current value equal to 6.1 A.

Figs. 12 and 13 show the experimental results obtained with the evolution of the speed, respectively, for flux-weakening algorithms with MTPV and conventional flux weakening. Finally, the best operation is obtained with the flux weakening and MTPV algorithm where the created torque is greater and al-

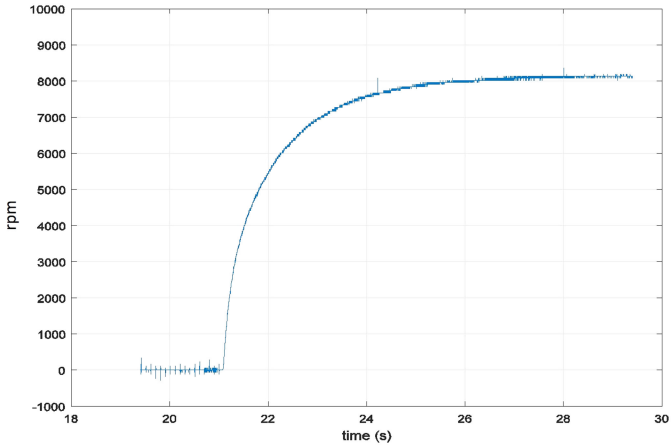

Fig. 12. Experimental evolution of rotation speed with flux weakening and MTPV.

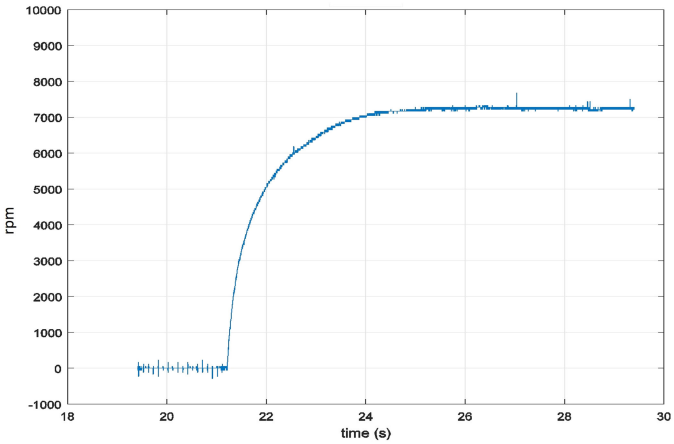

Fig. 13. Experimental evolution of rotation speed with classic weakening.

lows rotation speed equal to 8023 r/min to be reached. Classic flux weakening guarantees only 7227 r/min, a gain of 11% on previous solution. Thus, we confirm the high overspeed factor (8023/869 = 9.23) and the high flux-weakening level simultaneously.

All real-time control was implemented on *dSPACE* card (DS1104) (with master *Power PC* and DSP). A special field-programmable gate array card is added to accelerate the calculation of corrected PMSM position data.

VI. Conclusion

High speed PMSMs are used in electrical vehicles because they are lighter, smaller, and cheaper than other classic PMSM. The main point of operation of these machines at high speed is the flux-weakening method associated with a general control strategy. In this paper, the authors present a pertinent control strategy defined in the *d–q* reference frame that enables these machines to be driven whatever their speed. This strategy satisfies all constraints imposed by reference operating points such as: the voltage limit, the current limit, and the battery power limit. The flux weakening is carried out by a regulation of the reference voltage given by the current regulation and ensures that it does not go over the voltage limit.

So, if the critical point is within the current limitation, then the MTPV strategy is required to maximize the torque achievable at high speed with minimal current and respecting the voltage limit. This MPTV is taken into account in the control by modifying the current limit at high speed with the current required for MTPV in continuous mode and without needing to switch between algorithms. Finally, the performances of the proposed control are observed through simulations. They were also validated experimentally, and satisfactory concordances are observed in the different operating points between experimental and simulation results as shown in this paper.

Consequently, this study confirms that the proposed control strategy with flux weakening and MTPV globally improves the PMSM propulsion operation and especially improves the effectiveness of energy conversion. This study confirms that the control strategy has been improved and that the MTPV has increased the effectiveness of the PMSM with an overspeed regime of more than 9 and a speed increased by 10%.

References

[1] T. Finken, M. Felden, and K. Hameyer, "Comparison and design of different electrical machine types regarding their applicability in hybrid electrical vehicles," in *Proc. 18th Int. Conf. Elect. Mach.*, Vilamoura, Portugal, 2008, pp. 1–5.

[2] L. Sepulchre, M. Fadel, and M. Pietrzak-David, "Improvement of the digital control of a high speed PMSM for vehicle application," in *Proc. 11th Int. Conf. Ecological Veh. Renewable Energies*, Monte Carlo, Monaco, 2016, pp. 1–9.

[3] L. Dongyun and N. C. Kar, "A review of flux weakening control in permanent magnet synchronous machines," in *Proc. IEEE Veh. Power Propulsion Conf.*, Sep. 1–3, 2010, pp. 1–6.

[4] S. Bolognani, S. Calligaro, R. Petrella, and F. Pogni, "Flux weakening in IPM motor drives: Comparison of state-of-art algorithms and a novel proposal for controller design," in *Proc. 14th Eur. Conf. Power Electron. Appl.*, Aug. 30, 2011–Sep. 1, 2011, pp. 1–11.

[5] F. Gao, S. Bozhko, Y. S. Shen, and G. Asher, "Control design for PMM starter-generator operated in flux weakening mode," in *Proc. 48th Int. Univ. Power Eng. Conf.*, Sep. 2–5, 2013, pp. 1–6.

[6] Z. Fangyang, R. Feng, L. Jianjun, and H. Peng, "Study on flux weakening control for PMSM," in *Proc. 4th Int. Symp. Knowl. Acquisition Model.*, Oct. 8–9, 2011, pp. 192–195.

[7] S. Morimoto, M. Sanada, and Y. Takeda, "Wide-speed operation of interior permanent magnet synchronous motors with high-performance current regulator," *IEEE Trans. Ind. Appl.*, vol. 30, no. 4, pp. 920–926, Jul./Aug. 1994.

[8] T. Huber, W. Peters, and J. Böcker, "Voltage controller for flux weakening operation of interior permanent magnet synchronous motor in automotive traction applications," in *Proc. Int. Elect. Mach. Drives Conf.*, 2015, pp. 1078–1083.

[9] W. Peters, T. Huber, and J. Böcker, "Control realization for an interior permanent magnet synchronous motor (IPMSM) in automotive drive trains," in *Proc. Int. Exhib. Conf. Power Electron. Intell. Motion Renewable Energy Energy Manage.*, 2011, pp. 1–10.

[10] M. Meyer and J. Bocker, "Optimum control for interior permanent magnet synchronous motors (IPMSM) in constant torque and flux weakening range," in *Proc. 12th Int. Power Electron. Motion Control Conf.*, Aug. 30, 2006–Sep. 1, 2006, pp. 282–286.

[11] M. Meyer, T. Grote, and J. Bocker, "Direct torque control for interior permanent magnet synchronous motors with respect to optimal efficiency," in *Proc. Eur. Conf. Power Electron. Appl.*, Sep. 2–5, 2007, pp. 1–9.